Available online at www.sciencedirect.com
SCIENCE DIRECT®
ELSEVIER
International Journal of Multiphase Flow 31 (2005) 809–823
International Journal of Multiphase Flow
www.elsevier.com/locate/ijmulflow

# Effect of particle size distribution on pressure drop and concentration profile in pipeline flow of highly concentrated slurry

D.R. Kaushal [a,*], Kimihiko Sato [b], Takeshi Toyota [b], Katsuya Funatsu [b], Yuji Tomita [b]

[a] *Department of Civil Engineering, Indian Institute of Technology, Hauz Khas, New Delhi-110 016, India*
[b] *Department of Mechanical and Control Engineering, Kyushu Institute of Technology, 1-1 Sensui Cho, Tobata, Kitakyushu 804-8550, Japan*

Received 1 April 2003; received in revised form 6 March 2005

**Abstract**

The experiments were conducted in 54.9 mm diameter horizontal pipe on two sizes of glass beads of which mean diameter and geometric standard deviation are 440 μm & 1.2 and 125 μm & 1.15, respectively, and a mixture of the two sizes in equal fraction by mass. Flow velocity was up to 5 m/s and overall concentration up to 50% by volume for each velocity. Pressure drop and concentration profiles were measured. The profiles were obtained traversing isokinetic sampling probes in the horizontal, 45° inclined and vertical planes including the pipe axis. Slurry samples of the mixture collected in the vertical plane were analyzed for concentration profiles of each particle batch constituting the mixture. It was found that the pressure drop is decreased for the mixture at high concentrations except 5 m/s and a distinct change of concentration profiles was observed for 440 μm particles indicating a sliding bed regime, while the profiles in the horizontal plane remains almost constant irrespective of flow velocity, overall concentration and slurry type.


* Corresponding author. Tel.: +91 1126591216; fax: +91 1126581117.
*E-mail address:* kaushal@civil.iitd.ac.in (D.R. Kaushal).

0301-9322/$ - see front matter © 2005 Elsevier Ltd. All rights reserved.
doi:10.1016/j.ijmultiphaseflow.2005.03.003

*Keywords:* Highly concentrated slurry; Mixture of two particle sizes; Pressure drop; Concentration profiles in different planes; Concentration profiles of constituent particles

## 1. Introduction

Liquid–solid two phase flow is widely employed in the chemical and mining industries in slurry pipelines and is encountered in natural phenomena such as river mechanics. It has been the endeavour of researchers around the world to develop accurate models for pressure drop and concentration distribution in slurry pipeline. Pressure drop is one of the most important technical parameters to be evaluated by the designer for designing a pipeline slurry transportation system, and is the parameter, which dictates the selection of pump capacity. Several studies for pressure drop prediction in slurry flow are available in literature (Wasp et al., 1977; Doron et al., 1987; Gillies et al., 1991; Sundqvist et al., 1996; Mishra et al., 1998; Ghanta and Purohit, 1999; Wilson et al., 2002; Schaan et al., 2000; Kaushal and Tomita, 2002; Kumar et al., 2003, etc.). Concentration distribution may be used to determine the parameters of direct importance (mixture and solid flow rates) and the secondary effects such as wall abrasion and particle degradation. The recent works of Kaushal and Tomita (2002) and Kumar et al. (2003) are worth mentioning in the field of concentration distribution in slurry pipeline.

Most of the earlier studies on slurry pipeline systems are based on moderate volumetric concentrations of solids (say up to 26%). Much larger concentrations now coming into common use show more complicated behaviour. Also in any practical situation, the solids are coarser in size with broad particle grading being transported at large flow velocities. The flow characteristics of such slurries are studied experimentally in the present study, which will be analyzed to bring out the effect of particle size distribution on pressure drop and concentration profile.

## 2. Experimental equipment

A test loop was built to obtain flow rates, concentration profile, pressure drop and flow patterns. The test loop is laid horizontally in the Powder Technology Laboratory of KIT, Japan. A schematic layout and plan view along with the important dimensions of the rig are presented in Fig. 1. The pipe inside diameter is 54.9 mm. The rig consists of 22 m long recirculating pipe loop, 200 l capacity slurry tank, 150 l capacity water tank and a centrifugal pump to maintain the slurry flow. The pipe loop, slurry tank and water tank are fabricated with stainless steel. The slurry is supplied from the slurry tank (7 in Fig. 1(b)), where a mixer powered by an electric motor mixes the water and the solid particles mechanically. The rotation rate of the mixer is kept sufficiently high to obtain homogeneous solids distribution in the slurry tank. Sufficient care was taken to minimize the introduction of air bubbles into the system. The tank outlet is located approximately 10 cm above the bottom (approximately 10 cm below the mixer impeller). An additional water tank (10 in Fig. 1(b)) is connected parallel to the slurry tank as a buffer, so that the variations of the mixture level in the slurry tank at start-up and shut-down are reduced. The slurry is circulated through the system by a centrifugal pump (1 in Fig. 1(b)) with rubber coated recessed impeller. The pump was chosen to cover the expected range of operational conditions—15 kW

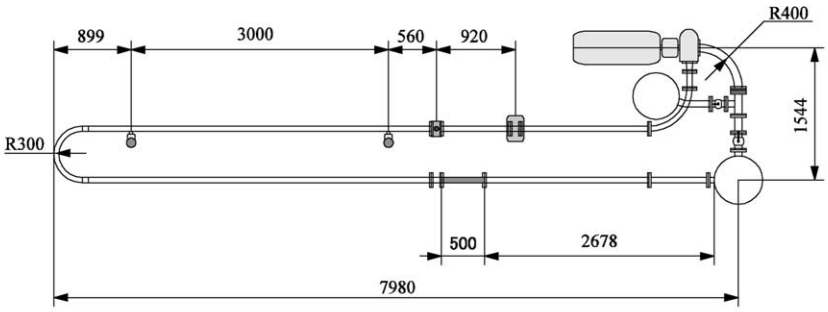


(a) Plan view (all the dimensions are in mm)

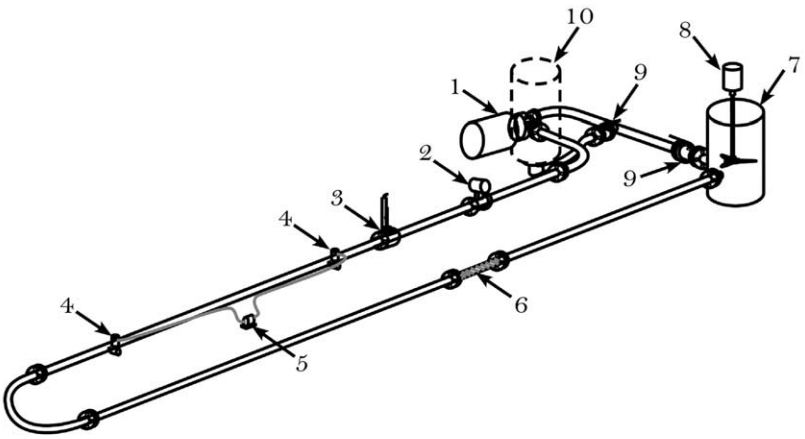


1. Slurry Pump 2. Electomagnetic flow meter 3. Isokinematic sampling probe
4. Pressure tapings 5. Differential pressure transducer 6. Observation chamber
7. Slurry Tank 8. Mixer 9. Valve 10. Water Tank

(b) Schematic diagram

Fig. 1. Test loop used in the present study.

pump, which supplies 0.6 $m^3$/min at 22 m head. The flow rate is controlled using frequency inverter, which enables adjustment of the rotational speed of the pump to any desired value.

The slurry volumetric flow rate is measured using an electromagnetic flow meter (2 in Fig. 1(b)).

A sampling probe (3 in Fig. 1(b)) to measure the concentration profile has a 5 mm × 6 mm rectangular slot 3 mm above the end. The concentration profiles in different planes were measured at corresponding flow velocity and overall concentration. Samples are collected from different locations in the horizontal, 45° inclined and vertical planes including pipe axis under near isokinetic flow conditions. During the collection of samples, it was ensured that the flow of the slurry through the sampling tube outlet is continuous and uniform. Sufficient time was allowed before sample collection to ensure steady state conditions. The sampling probe was mounted on vernier type of traversing mechanism.

The choice of two individual particle sizes was such that for mixture of two sizes, particle size distributions of different sizes do not overlap with each other. Thus, we can analyze the ratio of constituent particles in the mixture by using sieve having opening of intermediate diameter. Slurry samples for flow with the mixture in the vertical traversing were analyzed for fraction and concentration profile of constituent particles. The samples were divided into two classes by using a sieve of 300 μm. Thus, we could evaluate the distributions of constituent particle batches of 440 μm and 125 μm sizes in the mixture flow.

In this paper, the overall area-average concentration, $C_{vf}$, is used as characteristic concentration for each experiment, which is an area-averaged value of concentration by integrating the concentration profile measured by isokinetic sampling probe in the vertical plane. We planned the experiment so that the overall area-average concentration be equally spaced every 10% from 10% to 50%. The resulting $C_{vf}$ is given in the last row of Table 2(a), 2(b) and 2(c). The experimental results discussed in this paper are for such concentration groups.

The differential pressure is measured between two pressure measurement stations (4 in Fig. 1(b)) located 3 m apart. This constitutes a length of around 60 pipe diameters. These locations were chosen such that the end effects would be reduced as possible. Separation chambers along with pressure taps are provided at both the stations for ensuring that only water can enter into the pressure transducer and their tubings, and that solid particles are not stuck in the tap opening. Flexible transparent rubber tubes connect the taps to the differential pressure transducer. The differential pressure transducer covers the pressure up to 50 kPa.

The temperature of slurry was measured using copper–constantan thermo-couples (0.4 mm diameter) fixed at the back of the nickel chrome foil at circumferential fixed intervals of 10° and digital thermometer. The thermo-couples were installed in the pressure tappings.

The output signals from differential pressure transducer, thermo-couples and electromagnetic flow meter are recorded by data acquisition system. The readings were taken after the flow pattern was sufficiently stabilized (this was determined both by visual observation and by examining the trend of pressure drop and flow rate readings). Each data point was obtained by evaluation of the average of around 2000 readings.

In the straight pipeline, a small length (0.5 m) of perspex pipe (6 in Fig. 1(b)) was provided to establish the deposition velocity of the slurry in the pipeline by observing the motion of the particles at the bottom of the pipeline.

## 3. Material used and its properties

Spherical glass beads with mean diameters of 125 μm, 440 μm and a mixture of the two sizes have been used to prepare the slurry for the present study. The mixture was prepared by adding 125 μm and 440 μm particles in proportion of 50/50 by mass to the pipe loop. However, the mass ratio MR was not always 50/50 in the flow, and generally the coarser particle size circulated more in the pipeline, in particular, when the concentration is high, which is shown in Table 2(c). The average specific gravity was measured as 2.47. Particle size distributions in the fresh samples were determined by laser scattering analyser, which can measure the particle sizes in the range from 0.05 μm to 879 μm. The measured particle size distributions of three sets of particles are shown in Fig. 2. The distributions for both the sizes (i.e., 125 μm and 440 μm) were found to

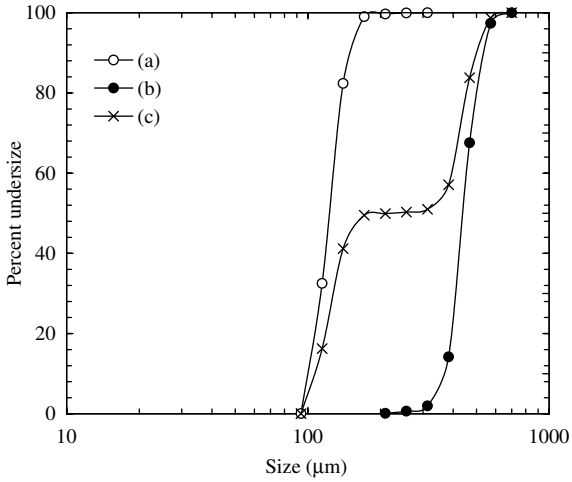


Fig. 2. Particle size distribution of different particles used in the present study. (a) $d_m = 125$ mm, $\sigma_g = 1.15$. (b) $d_m = 440$ mm, $\sigma_g = 1.20$. (c) Mixture of two sizes in equal fraction by mass.

be log-normal. The scatter of a log-normal distribution is usually defined by the geometric standard deviation $\sigma_g$ determined from the property that the value of the distributed variable corresponding to a cumulative probability of 84.1% is $\sigma_g$ times the geometric mean. Thus, monodisperse particles have $\sigma_g = 1$, while particle size distributions with $\sigma_g$ less than about 1.5 are usually considered to be narrowly sized. If we apply the log-normal distribution, the deviations $\sigma_g$ for 125 μm and 440 μm were found to be 1.15 and 1.2 respectively, indicating narrow distributions.

## 4. Experimental results

The measurement was done by monotonously increasing or decreasing flow velocity, $V_m$, for a given particle concentration. It took about 7 min to complete measurement for a given flow velocity and concentration. The temperature rise during measurement was large when the particle size was 440 μm and the flow velocity was high, but was weakly dependent on the concentration. The overall average temperature rise was about one degree at most between measurements. During the measurement we did not identify any monotonous trend of the readings in pressure drop and flow rate.

### 4.1. Pressure drop

Figs. 3–5 show the pressure drop per unit length $\Delta p/l$ against flow velocity $V_m$ and the results are tabulated in Table 1. To check the accuracy of the experimental pressure drop in the flow of water, the results were compared with the Moody's chart. Water data were found to follow the Moody's chart corresponding to zero relative roughness. The velocity is varied between the maximum achievable value and the minimum possible velocity, where particles start to settle at the bottom of the pipe, for all the concentrations of different slurries. The flow velocity at which the solid

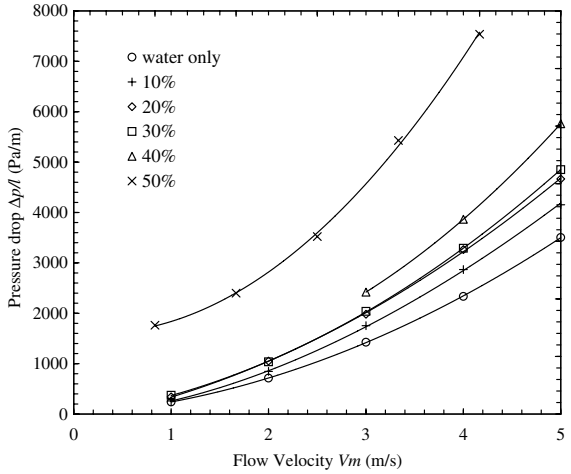


Fig. 3. Pressure drop for slurry of 125 μm particle size at different overall area-average concentrations and flow velocities.

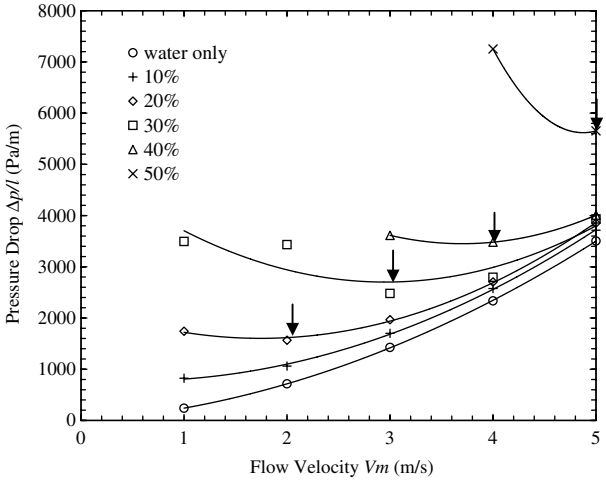


Fig. 4. Pressure drop for slurry of 440 μm particle size at different overall area-average concentrations and flow velocities.

particles are in rolling motion at the bottom of the pipe is taken as "streaking at the bottom". Further reduction in the flow velocity results in the bottom-most particles coming to rest and this velocity is termed the deposition/critical velocity. In Figs. 4 and 5, deposition velocity is indicated using arrow mark and the corresponding values of pressure drop are indicated in Table 1. At still lower velocities, the movement of particles occurs as a bed at bottom of the pipe and is identified as the moving bed velocity. Below this velocity, a static bed is formed and final choking of the pipe takes place as the bed thickness increases to cover the total pipe cross-section.

Pressure drop for slurry of 125 μm particles are presented in Fig. 3 at overall area-average concentrations around 10%, 20%, 30%, 40% and 50%. It is observed that the pressure drop at any

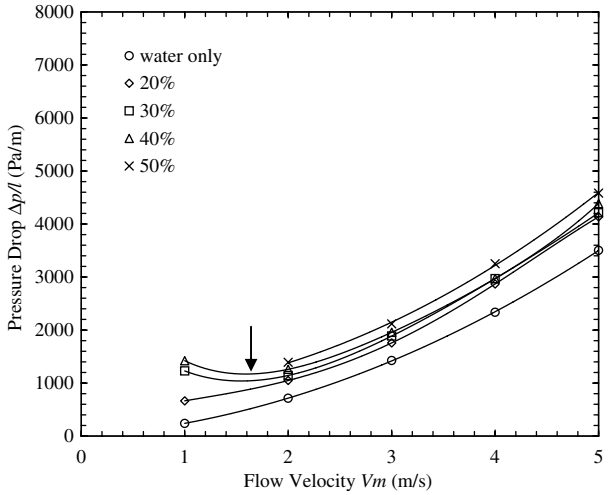


Fig. 5. Pressure drop for slurry of the mixture of 125 μm and 440 μm particle sizes at different overall area-average concentrations and flow velocities.

Table 1(a)
Pressure drop in Pa/m for 125 μm particles

| $V_m$ (m/s) | $C_{vf}$ | $\Delta p/l$ (Pa/m) | $C_{vf}$ (%) | $\Delta p/l$ (Pa/m) | $C_{vf}$ (%) | $\Delta p/l$ (Pa/m) | $C_{vf}$ (%) | $\Delta p/l$ (Pa/m) | $C_{vf}$ (%) | $\Delta p/l$ (Pa/m) |
|---|---|---|---|---|---|---|---|---|---|---|
| 1 | 9.4 | 261 | 19.22 | 341 | 30.3 | 373 | | | | 1543 |
| 2 | 10.06 | 847 | 20.48 | 1051 | 30.02 | 1037 | 41.1 | | 51.7 | 2099 |
| 3 | 10.41 | 1754 | 20.4 | 1981 | 31.19 | 2037 | 38.95 | 2420 | 49.24 | 3082 |
| 4 | 10.44 | 2868 | 19.52 | 3263 | 30.75 | 3291 | 40.64 | 3865 | 48.56 | 4750 |
| 5 | 10.93 | 4153 | 20.45 | 4666 | 30.24 | 4851 | 39.56 | 5761 | 48.96 | 6595 |

Table 1(b)
Pressure drop in Pa/m for 440 μm particles

| $V_m$ (m/s) | $C_{vf}$ (%) | $\Delta p/l$ (Pa/m) | $C_{vf}$ (%) | $\Delta p/l$ (Pa/m) | $C_{vf}$ (%) | $\Delta p/l$ (Pa/m) | $C_{vf}$ (%) | $\Delta p/l$ (Pa/m) | $C_{vf}$ (%) | $\Delta p/l$ (Pa/m) |
|---|---|---|---|---|---|---|---|---|---|---|
| 1 | 9.77 | 824 | 22.29 | 1742 | 33.91 | 3495 | | | | |
| 2 | 8.54 | 1061 | 21.13 | 1567 | 32.31 | 3433 | | | | |
| 3 | 9.39 | 1700 | 21.68 | 1966 | 30.01 | 2478 | 41.59 | 3614 | | |
| 4 | 10.38 | 2576 | 20.12 | 2705 | 30.02 | 2794 | 42.47 | 3480 | 48.97 | 7253 |
| 5 | 8.62 | 3715 | 18.77 | 3854 | 30.7 | 3934 | 41.18 | 4009 | 49.67 | 5652 |

given flow velocity increases with increase in concentration. This trend is seen for all concentrations at all velocities. The rate of increase in pressure with concentration is small at low velocities but it increases rapidly at higher velocities. The pressure drop for slurry of 440 μm particles are presented in Fig. 4 at overall area-average concentrations around 10%, 20%, 30%, 40%, and 50%. From this figure, it is observed that the pressure drop at any given flow velocity increases with increase in concentration, but the rate of increase is comparatively smaller at higher flow

Table 1(c)
Pressure drop in Pa/m for mixture of 125 μm and 440 μm particles

| $V_m$ (m/s) | $C_{vf}$ (%) | $\Delta p/l$ (Pa/m) | $C_{vf}$ (%) | $\Delta p/l$ (Pa/m) | $C_{vf}$ (%) | $\Delta p/l$ (Pa/m) | $C_{vf}$ (%) | $\Delta p/l$ (Pa/m) |
|---|---|---|---|---|---|---|---|---|
| 1 | 20.18 | 665 | 31.17 | 1229 | 38.98 | 1422 | | |
| 2 | 17.71 | 1048 | 30.43 | 1143 | 40.56 | 1260 | 48.64 | 1392 |
| 3 | 18.38 | 1757 | 29.22 | 1886 | 38.51 | 1957 | 47.85 | 2117 |
| 4 | 20.92 | 2869 | 30.3 | 2970 | 38.04 | 2971 | 48.46 | 3251 |
| 5 | 19.73 | 4136 | 30.49 | 4212 | 39.03 | 4386 | 48.89 | 4583 |

velocities. Furthermore, at lower velocities, pressure drop remains constant at lower concentrations and decreases with flow velocity at higher concentrations. At the largest concentration (i.e., 50%), the pressure drop decreases with flow velocity even up to the largest flow velocity of 5 m/s. From Figs. 3 and 4, it is observed that finer particle size has less pressure drop at lower flow velocities and has more pressure drop at higher flow velocities than coarser particles. Such an increase in pressure drop for coarser particle size at lower velocity is due to the increased amount of particles moving in the bed due to gravitational effect, while, in case of finer particle size at higher velocities, pressure drop is more due to greater surface area causing more frictional losses in suspension. Fig. 5 depicts the pressure drop for the mixture of 125 μm and 440 μm particles at overall concentrations around 20%, 30%, 40% and 50%. From Figs. 3–5, it is observed that for mixture of two sizes pressure drop is less for most of the observations at higher overall concen-

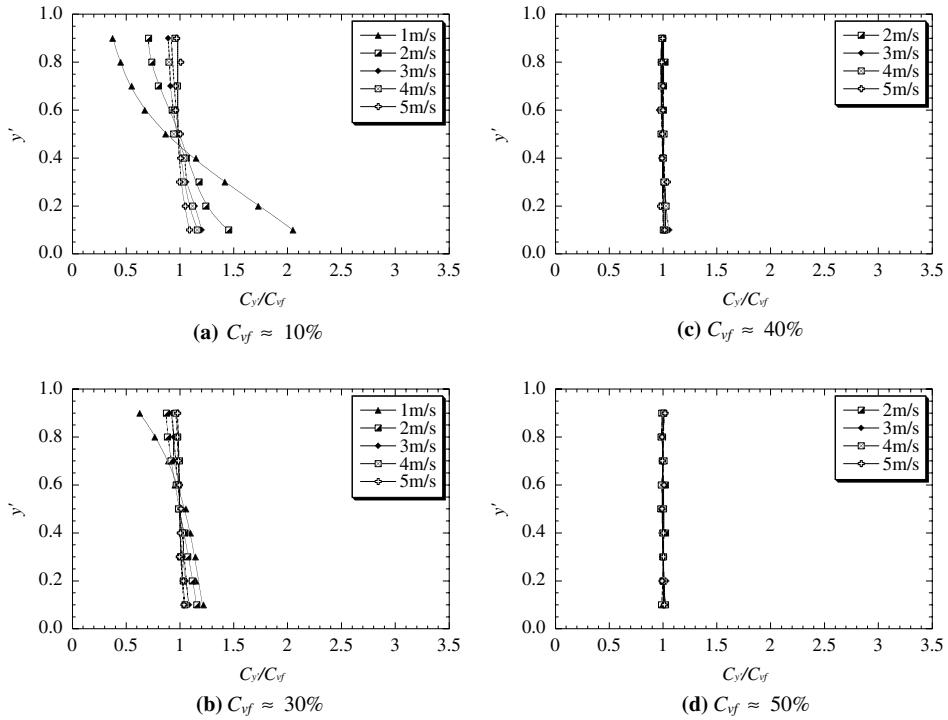


Fig. 6. Concentration profiles in the vertical plane for slurry of 125 μm particle size.

trations, except for 5 m/s. It may be partly due to the fact that the smaller particles prevent the larger particles from forming a moving bed by impinging.

### 4.2. Solids concentration profiles

Figs. 6–8 show concentration profiles in the vertical plane for slurry of 125 μm, 440 μm and the mixture of the two particle sizes, respectively, by $C_{y'}/C_{vf}$ vs. $y'$, where $C_{y'}$ is the volumetric concentration at $y' = y/D$, $y$ being distance from the pipe bottom and $D$ the pipe diameter. Table 2 summarises the result.

It is observed that the particles are asymmetrically distributed in the vertical plane with the degree of asymmetry increasing with increase in particle size because of the gravitational effect. It is also observed that the degree of asymmetry for the same overall concentration of slurry increases with decreasing flow velocity. This is expected because with decrease in flow velocity there will be a decrease in turbulent energy, which is responsible for keeping the solids in suspension. From these figures, it is also observed that for a given velocity, increasing concentration reduces the asymmetry because of enhanced interference effect between solid particles. The effect of this interference is so strong that the asymmetry even at lower velocities is very much reduced at higher concentrations. Therefore it can be concluded that degree of asymmetry in the concentration

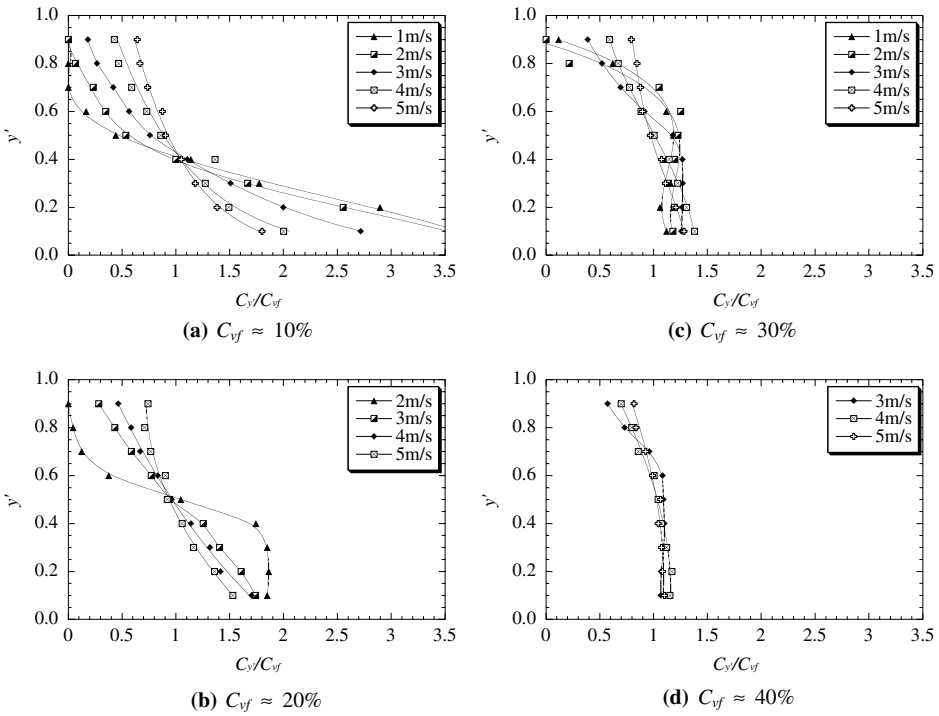


Fig. 7. Concentration profiles in the vertical plane for slurry of 440 μm particle size.

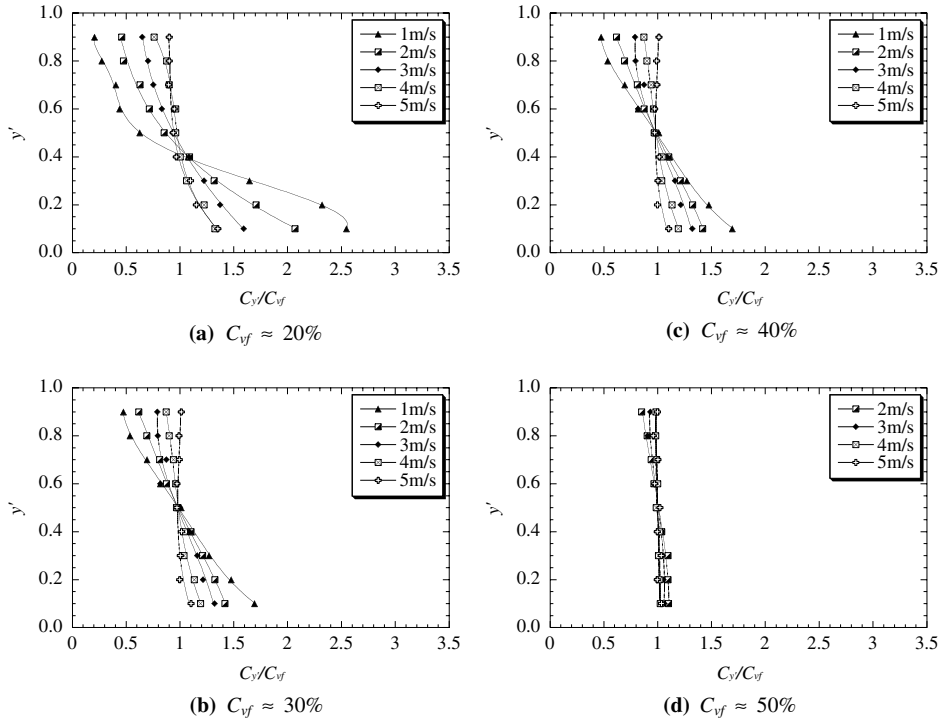


Fig. 8. Concentration profiles in the vertical plane for the mixture of 125 μm and 440 μm particle sizes.

profiles in the vertical plane depends upon the particle size, velocity of flow and overall concentration of slurry.

Measured concentration profiles show a distinct change in the shape for slurries of coarser particle size (i.e., 440 μm) with higher concentrations at lower velocities. It is observed that the maximum concentration at bottom does not change and extends up to centre of the pipeline, thus making a sudden drop in the concentration in the upper half of the pipeline. The reason for such a distinct change in shape of concentration profiles may be attributed to the sliding bed regime for coarser particles at lower velocities and higher concentrations.

The typical measured concentration profiles in the 45° inclined plane, $C_{z'}/C_{\mathrm{vf}}$ vs. $z'$ ($C_{z'}$ is the volumetric concentration at $z' = z/D$, where $z$ is the distance from the lower side along the traversing diameter in the inclined plane) are shown in Fig. 9, for slurry of 125 μm, 440 μm and the mixture of the two particle sizes at different overall concentrations and flow velocities. The trends obtained were fairly matching with those obtained in the vertical plane.

The typical measured concentration profiles in the horizontal plane, $C_{x'}/C_{\mathrm{vf}}$ vs. $x'$ ($C_{x'}$ is the volumetric concentration at $x' = x/D$, $x$ is the distance from the pipe wall along the horizontal diameter) are shown in Fig. 10, for slurry of 125 μm, 440 μm and the mixture of the two particle sizes, respectively, at different overall concentrations and flow velocities. From these figures, it is observed that the concentration in the horizontal plane remains almost uniform irrespective of particle size, flow velocity and overall concentration. The trend at all the overall concentrations and flow velocities remains almost similar.

Table 2(a)
Concentration profiles in vertical plane for 125 μm particles

| $y'$ | Flow velocity $V_m$ (m/s) | | | | | Flow velocity $V_m$ (m/s) | | | | | Flow velocity $V_m$ (m/s) | | | | | Flow velocity $V_m$ (m/s) | | | | Flow velocity $V_m$ (m/s) | | | |
|---|---|---|---|---|---|---|---|---|---|---|---|---|---|---|---|---|---|---|---|---|---|---|---|
| | 1 | 2 | 3 | 4 | 5 | 1 | 2 | 3 | 4 | 5 | 1 | 2 | 3 | 4 | 5 | 2 | 3 | 4 | 5 | 2 | 3 | 4 | 5 |
| 0.1 | 19.28 | 14.61 | 12.50 | 12.13 | 11.91 | 28.69 | 23.70 | 21.28 | 21.13 | 21.25 | 36.94 | 34.70 | 33.84 | 32.19 | 31.37 | 41.20 | 41.19 | 41.42 | 40.24 | 50.97 | 49.66 | 49.71 | 49.54 |
| 0.2 | 16.24 | 12.47 | 11.85 | 11.66 | 11.46 | 24.55 | 22.44 | 22.00 | 20.08 | 20.59 | 34.81 | 33.45 | 32.86 | 31.68 | 31.14 | 40.76 | 39.69 | 41.76 | 38.63 | 51.78 | 50.72 | 48.54 | 48.53 |
| 0.3 | 13.33 | 11.84 | 11.02 | 10.74 | 10.87 | 23.46 | 21.86 | 20.59 | 19.83 | 20.94 | 34.67 | 32.18 | 31.90 | 30.89 | 30.00 | 41.48 | 39.52 | 41.04 | 41.10 | 51.52 | 48.87 | 48.74 | 49.13 |
| 0.4 | 10.81 | 10.64 | 10.89 | 10.82 | 11.01 | 18.06 | 21.24 | 20.39 | 20.16 | 20.65 | 33.25 | 31.40 | 32.43 | 31.49 | 30.32 | 40.99 | 39.30 | 40.73 | 39.17 | 52.92 | 48.54 | 48.40 | 49.21 |
| 0.5 | 8.15 | 9.83 | 10.10 | 9.84 | 10.95 | 19.74 | 20.49 | 20.41 | 19.33 | 20.67 | 31.97 | 29.68 | 30.93 | 30.31 | 30.52 | 40.32 | 38.57 | 41.04 | 39.32 | 50.67 | 48.60 | 48.83 | 48.47 |
| 0.6 | 6.33 | 9.33 | 9.77 | 9.92 | 10.51 | 17.53 | 19.67 | 20.67 | 19.45 | 20.00 | 28.86 | 28.96 | 31.23 | 30.21 | 30.06 | 41.22 | 37.49 | 40.00 | 39.58 | 52.82 | 49.62 | 47.81 | 49.41 |
| 0.7 | 5.18 | 8.05 | 9.49 | 10.20 | 10.49 | 15.62 | 19.24 | 19.86 | 18.98 | 19.65 | 27.07 | 27.51 | 29.33 | 30.57 | 29.85 | 41.25 | 39.20 | 39.93 | 39.51 | 51.37 | 49.05 | 49.05 | 48.59 |
| 0.8 | 4.22 | 7.42 | 9.40 | 9.36 | 11.02 | 14.35 | 18.04 | 19.18 | 18.20 | 20.17 | 23.21 | 26.49 | 29.38 | 30.06 | 29.56 | 41.83 | 38.10 | 39.93 | 39.09 | 51.46 | 49.15 | 47.67 | 48.44 |
| 0.9 | 3.52 | 7.13 | 9.27 | 9.94 | 10.60 | 12.63 | 17.90 | 18.96 | 18.88 | 20.47 | 18.97 | 26.27 | 28.80 | 29.51 | 29.63 | 41.03 | 38.43 | 40.15 | 39.51 | 51.08 | 49.73 | 48.92 | 49.84 |
| $C_{vf}$ | 9.40 | 10.06 | 10.41 | 10.44 | 10.93 | 19.22 | 20.48 | 20.40 | 19.52 | 20.45 | 30.30 | 30.02 | 31.19 | 30.75 | 30.24 | 41.10 | 38.95 | 40.64 | 39.56 | 51.70 | 49.24 | 48.56 | 48.96 |

Table 2(b)
Concentration profiles in vertical plane for 440 μm particles

| $y'$ | Flow velocity $V_m$ (m/s) | | | | | Flow velocity $V_m$ (m/s) | | | | | Flow velocity $V_m$ (m/s) | | | | | Flow velocity $V_m$ (m/s) | | | Flow velocity $V_m$ (m/s) | |
|---|---|---|---|---|---|---|---|---|---|---|---|---|---|---|---|---|---|---|---|---|
| | 1 | 2 | 3 | 4 | 5 | 1 | 2 | 3 | 4 | 5 | 1 | 2 | 3 | 4 | 5 | 3 | 4 | 5 | 4 | 5 |
| 0.1 | 35.26 | 30.09 | 25.52 | 20.77 | 15.52 | 37.14 | 39.05 | 37.71 | 34.32 | 28.72 | 38.02 | 38.08 | 37.76 | 41.46 | 39.36 | 44.38 | 48.93 | 45.26 | 48.74 | 51.67 |
| 0.2 | 28.30 | 21.79 | 18.75 | 15.49 | 11.92 | 38.43 | 39.36 | 34.81 | 28.46 | 25.50 | 35.99 | 38.55 | 38.03 | 39.17 | 37.12 | 44.47 | 49.67 | 44.57 | 48.54 | 50.67 |
| 0.3 | 17.35 | 14.23 | 14.15 | 13.21 | 10.17 | 34.07 | 39.05 | 30.45 | 26.49 | 21.82 | 39.26 | 36.75 | 38.10 | 36.74 | 34.06 | 45.54 | 47.57 | 44.29 | 49.39 | 51.29 |
| 0.4 | 11.14 | 8.55 | 10.38 | 14.17 | 9.03 | 31.17 | 36.87 | 27.21 | 22.94 | 19.87 | 37.87 | 38.64 | 38.08 | 34.35 | 32.97 | 45.79 | 45.56 | 42.91 | 48.45 | 51.49 |
| 0.5 | 4.33 | 4.58 | 7.14 | 8.92 | 7.80 | 23.59 | 22.12 | 20.43 | 19.33 | 17.29 | 40.16 | 39.63 | 35.39 | 30.15 | 29.77 | 45.38 | 44.26 | 43.87 | 50.00 | 51.82 |
| 0.6 | 1.62 | 2.98 | 5.31 | 7.57 | 7.52 | 18.70 | 7.95 | 16.75 | 16.74 | 16.92 | 37.95 | 40.46 | 27.49 | 26.53 | 27.44 | 45.10 | 42.61 | 40.74 | 48.62 | 49.14 |
| 0.7 | 0.00 | 1.97 | 3.93 | 6.12 | 6.36 | 9.69 | 2.64 | 12.72 | 13.43 | 14.38 | 35.56 | 33.94 | 20.84 | 23.28 | 26.88 | 39.91 | 36.46 | 38.22 | 49.16 | 50.93 |
| 0.8 | 0.00 | 0.57 | 2.50 | 4.86 | 5.73 | 2.69 | 0.95 | 9.38 | 11.78 | 13.33 | 21.08 | 7.01 | 15.64 | 20.14 | 25.95 | 30.40 | 33.84 | 34.48 | 48.80 | 44.78 |
| 0.9 | 0.00 | 0.00 | 1.72 | 4.44 | 5.51 | 0.85 | 0.00 | 6.13 | 9.38 | 13.91 | 4.04 | 0.00 | 11.69 | 17.78 | 24.35 | 23.84 | 29.67 | 33.70 | 48.70 | 41.30 |
| $C_{vf}$ | 9.77 | 8.54 | 9.39 | 10.38 | 8.62 | 22.29 | 21.13 | 21.68 | 20.12 | 18.77 | 33.91 | 32.31 | 30.01 | 30.02 | 30.70 | 41.59 | 42.47 | 41.18 | 48.97 | 49.67 |

Table 2(c)
Concentration profiles in vertical plane for mixture of 125 μm and 440 μm particles

| $y'$ | Flow velocity $V_m$ (m/s) | | | | | Flow velocity $V_m$ (m/s) | | | | | Flow velocity $V_m$ (m/s) | | | | | Flow velocity $V_m$ (m/s) | | | |
|---|---|---|---|---|---|---|---|---|---|---|---|---|---|---|---|---|---|---|---|
| | 1 | 2 | 3 | 4 | 5 | 1 | 2 | 3 | 4 | 5 | 1 | 2 | 3 | 4 | 5 | 2 | 3 | 4 | 5 |
| 0.1 | 51.37 | 36.65 | 29.28 | 27.69 | 26.67 | 52.80 | 43.16 | 38.59 | 36.07 | 33.59 | 51.88 | 49.74 | 45.22 | 42.32 | 42.14 | 53.52 | 50.83 | 49.52 | 50.59 |
| 0.2 | 46.83 | 30.23 | 25.24 | 25.60 | 22.71 | 46.03 | 40.30 | 35.46 | 34.36 | 30.38 | 51.36 | 47.34 | 42.74 | 40.68 | 39.14 | 53.25 | 50.45 | 49.13 | 48.70 |
| 0.3 | 33.22 | 23.32 | 22.48 | 22.17 | 21.67 | 39.56 | 36.80 | 33.90 | 31.40 | 30.56 | 51.87 | 46.98 | 40.09 | 40.67 | 38.35 | 53.23 | 50.16 | 48.76 | 50.53 |
| 0.4 | 21.69 | 19.30 | 19.92 | 20.95 | 19.02 | 34.72 | 33.53 | 31.82 | 31.56 | 30.93 | 46.29 | 43.62 | 39.54 | 38.49 | 39.71 | 50.50 | 49.58 | 49.38 | 48.63 |
| 0.5 | 12.64 | 15.11 | 17.14 | 20.08 | 18.48 | 31.51 | 29.72 | 29.23 | 29.32 | 29.62 | 45.19 | 41.39 | 38.60 | 37.70 | 39.03 | 48.27 | 48.42 | 47.75 | 49.88 |
| 0.6 | 8.85 | 12.66 | 15.27 | 20.09 | 18.67 | 25.46 | 26.61 | 23.90 | 29.09 | 29.65 | 31.66 | 38.77 | 38.04 | 37.03 | 39.52 | 46.97 | 46.46 | 48.52 | 47.50 |
| 0.7 | 8.17 | 11.15 | 13.84 | 18.80 | 17.65 | 21.66 | 24.67 | 25.56 | 28.42 | 30.31 | 27.60 | 35.46 | 36.06 | 36.50 | 38.05 | 45.67 | 46.25 | 47.99 | 49.00 |
| 0.8 | 5.53 | 8.40 | 12.92 | 18.33 | 17.75 | 16.67 | 21.01 | 23.20 | 27.27 | 30.21 | 20.55 | 31.63 | 33.90 | 34.74 | 38.04 | 43.85 | 43.38 | 47.53 | 46.86 |
| 0.9 | 4.14 | 8.11 | 11.95 | 15.90 | 17.72 | 14.81 | 18.77 | 23.10 | 26.42 | 30.88 | 19.72 | 27.91 | 32.69 | 34.65 | 38.07 | 41.38 | 44.62 | 47.66 | 48.74 |
| MR* | 44.9/ | 46.3/ | 50.7/ | 55.8/ | 55.0/ | 49.5/ | 52.8/ | 56.2/ | 55.9/ | 54.5/ | 54.5/ | 57.1/ | 60.5/ | 59.9/ | 57.6/ | 55.7/ | 55.7/ | 57.2/ | 54.8/ |
| | 55.1 | 53.7 | 49.3 | 44.2 | 45.0 | 50.5 | 47.2 | 43.8 | 44.1 | 45.5 | 45.5 | 42.9 | 39.5 | 40.1 | 42.4 | 44.3 | 44.3 | 42.8 | 45.2 |
| $C_{vf}$ | 20.18 | 17.71 | 18.38 | 20.92 | 19.73 | 31.17 | 30.43 | 29.22 | 30.30 | 30.49 | 38.98 | 40.56 | 38.51 | 38.04 | 39.03 | 48.64 | 47.85 | 48.46 | 48.89 |

* MR is the mass ratio of 440 μm particles to that of 125 μm particles in flow.

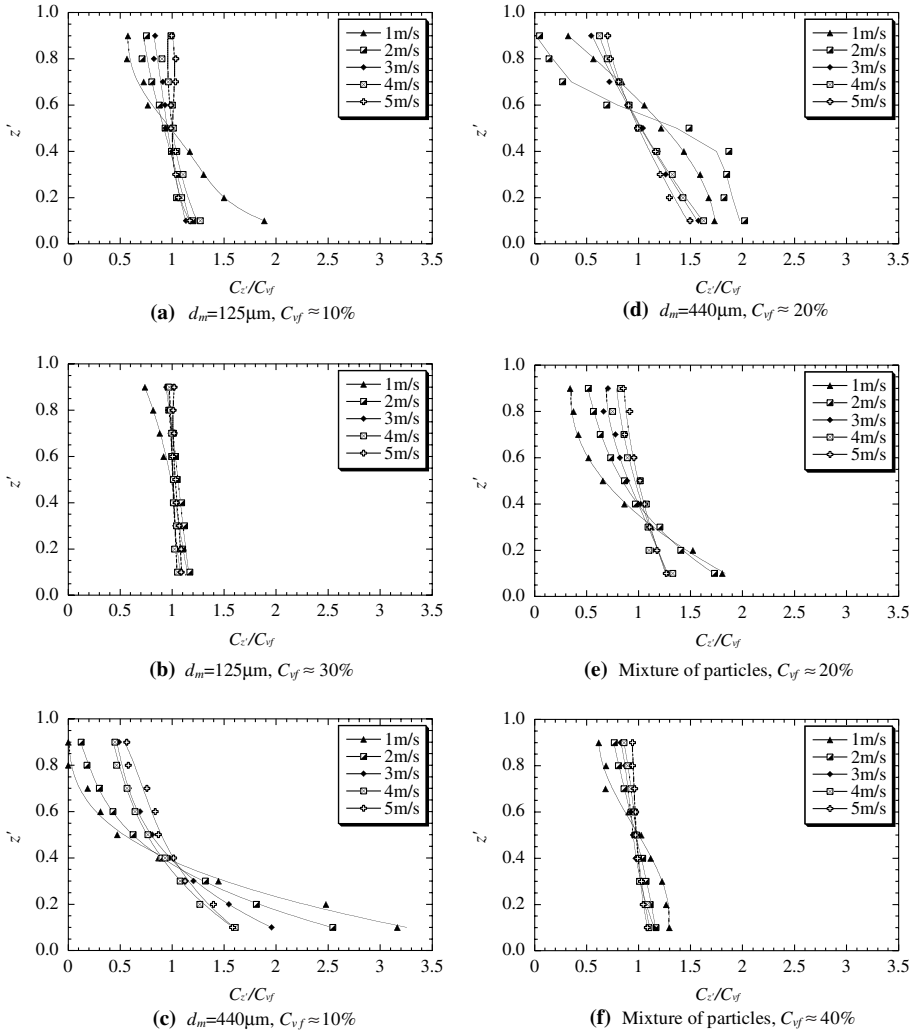


Fig. 9. Typical concentration profiles in the 45° inclined plane.

On the basis of putting together the concentration profiles in the 45° inclined and vertical planes, it is observed that the concentration in any horizontal plane remains constant. Thus the concentration distribution is considered as two-dimensional with fair degree of accuracy.

Fig. 11 shows the concentration profiles of constituent particles for flow with the mixture of two sizes in the vertical plane by $C_{y'j}/C_{\mathrm{vf}j}$ vs. $y'$, where $C_{y'j}$ is the concentration of $j$th batch particle in the mixture at $y'$ and $C_{\mathrm{vf}j}$ is the overall area-average concentration of that size particles. Generally, we expect $C_{y'j}/C_{\mathrm{vf}j}$ to increase from top to bottom of the pipe. Further, for coarser size fraction, the ratio $C_{y'j}/C_{\mathrm{vf}j}$ varies considerably. It is observed that the values of $C_{y'j}/C_{\mathrm{vf}j}$ is almost unity at all heights for 125 μm size particle for all concentrations and velocities tested except near the deposition velocity, thereby indicating this particle size distributed

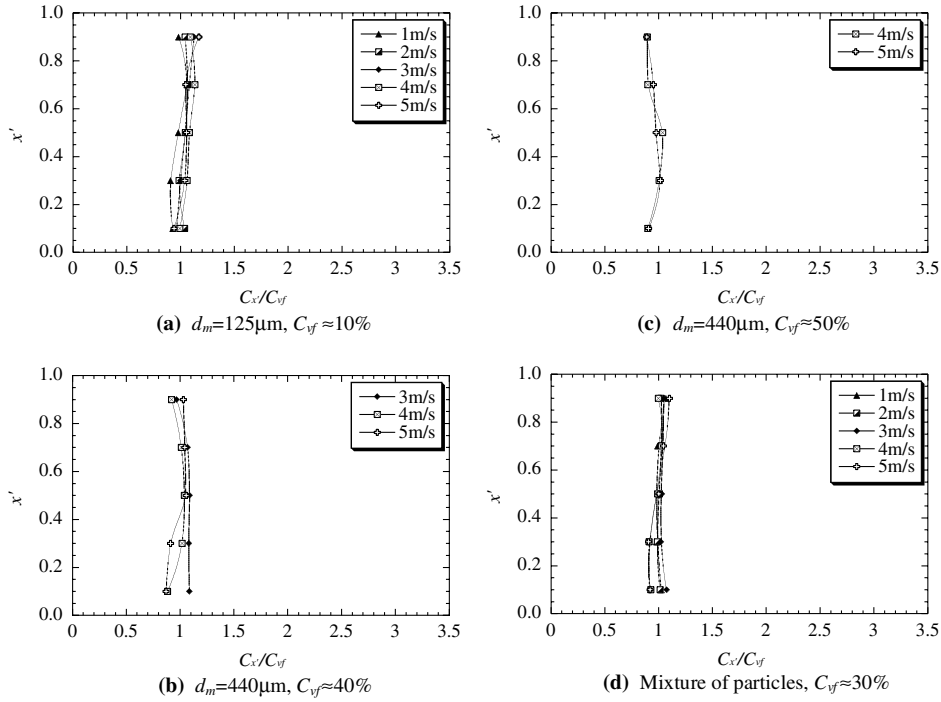


Fig. 10. Typical concentration profiles in the horizontal plane.

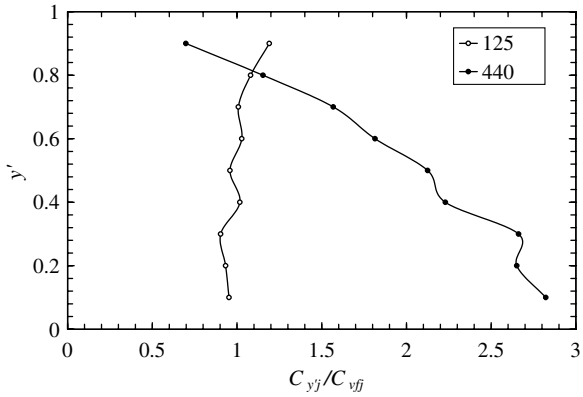


Fig. 11. Typical concentration profiles of constituent particle batch in the mixture of 125 μm and 440 μm particle sizes in the vertical plane.

homogeneously across the pipe cross section. The another size fraction (i.e. 440 μm) is asymmetrically distributed with the degree of asymmetry increasing with decrease in concentration and flow velocity.

## 5. Conclusions

Following conclusions have been drawn on the basis of present study:

1. The particle concentration profile is measured for high concentration slurry transport where the maximum overall area-average concentration is 50% by volume employing coarse particles and higher flow velocities up to 5 m/s.
2. Narrow grading particles tend to have high frictional losses, while broad grading particles have low frictional losses at high concentrations.
3. Concentration in the horizontal plane remains almost constant irrespective of flow velocity and overall concentration.
4. A distinct change in the shape of concentration profiles was observed indicating the sliding bed regime for coarser particles at lower flow velocities.

## References

Doron, P., Granica, D., Barnea, D., 1987. Slurry flow in horizontal pipes—Experimental and modeling. Int. J. Multiphase Flow 13, 535–547.

Ghanta, K.C., Purohit, N.K., 1999. Pressure drop prediction in hydraulic transport of bi-dispersed particles of coal and copper ore in pipeline. Can. J. Chem. Eng. 77, 127–131.

Gillies, R.G., Shook, C.A., Wilson, K.C., 1991. An improved two layer model for horizontal slurry pipeline flow. Can. J. Chem. Eng. 69, 173–178.

Kaushal, D.R., Tomita, Y., 2002. Solids concentration profiles and pressure drop in pipeline flow of multisized particulate slurries. Int. J. Multiphase Flow 28, 1697–1717.

Kumar, U., Mishra, R., Singh, S.N., Seshadri, V., 2003. Effect of particle gradation on flow characteristics of ash disposal pipelines. Powder Technol. 132, 39–51.

Mishra, R., Singh, S.N., Seshadri, V., 1998. Improved model for prediction of pressure drop and velocity field in multisized particulate slurry flow through horizontal pipes. Powder Handling and Processing Journal 10, 279–289.

Schaan, J., Sumner, R.J., Gillies, R.G., Shook, C.A., 2000. The effect of particle shape on pipeline friction for Newtonian slurries of fine particles. Can. J. Chem. Eng. 78, 717–725.

Sundqvist, A., Sellgren, A., Addie, G., 1996. Slurry pipeline friction losses for coarse and high density products. Powder Technol. 89, 19–28.

Wasp, E.J., Kenny, J.P., Gandhi, R.L., 1977. Solid Liquid Flow Slurry Pipeline Transportation, first ed. Trans. Tech. Publications, Clausthal, Germany.

Wilson, K.C., Clift, R., Sellgren, A., 2002. Operating points for pipelines carrying concentrated heterogeneous slurries. Powder Technol. 123, 19–24.